Effect of Lead Thickness on the BCAL Performance

S. Katsaganis, Z. Papandreou

Department of Physics, University of Regina, Regina, SK, S4S 0A2, Canada

Abstract

The GlueX experiment's electromagnetic barrel calorimeter should detect photons as low as 40 MeV and as high as 2 GeV. Moreover, the amount of light produced in its scintillating fibers should be as high as possible for a photon of a given energy, while preserving an adequate number of radiation lengths. To this end, Monte Carlo studies have been carried out and show that modest gains in threshold and light collection can be delivered, using 0.3 mm lead sheets instead of the nominal 0.5 mm sheets. Results on energy resolution, fractional energy deposition, as well as shower profile development and energy leakage are shown.

Key words: longitudinal shower profile, energy resolution, fractional deposition

Email addresses: st.katsaganis@gmail.com (S. Katsaganis),
zisis@uregina.ca (Z. Papandreou).

1 Introduction
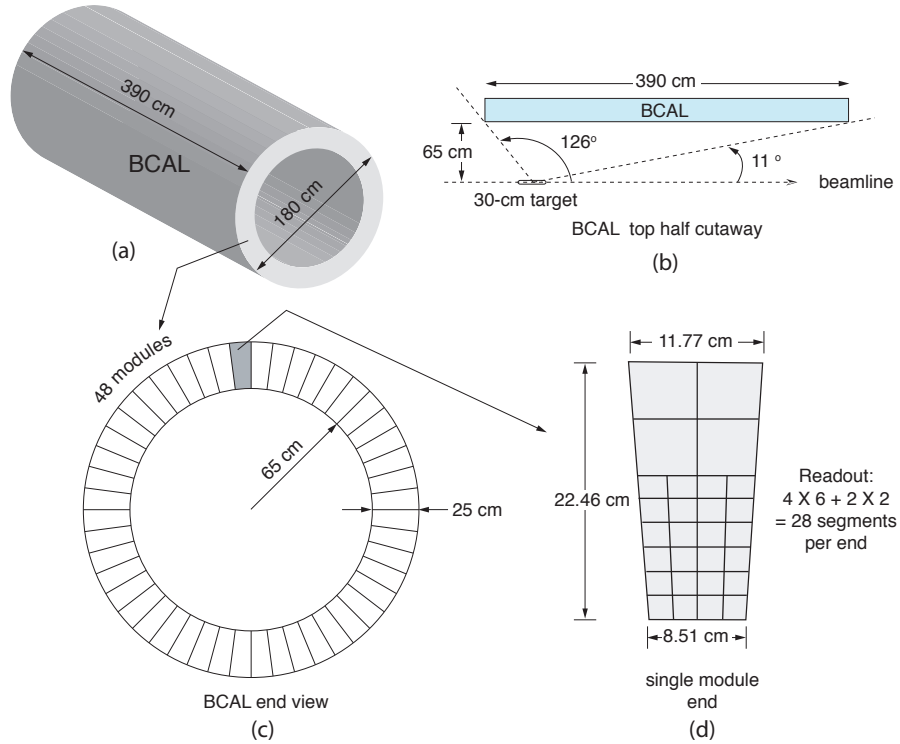
Fig. 1. General geometrical attributes of the BCAL and it's modules.

The BCAL consists of forty eight modules, each one having trapezoidal cross-sectional area on the x-y plane and a length of four meters on the z-axis; its geometrical configuration is shown in Figure 1. Each module is made of layers of scintillating fibers, sandwiched between sheets of lead. The lead sheets undergo mechanical deformation to support the fibers and also to prevent fibers from being glued at an arbitrary position between the lead sheets. After the sheets have been swaged, the fibers are positioned and the layer and the fibers are bonded to the next layer using optical epoxy. This process results in a module with well defined geometrical dimensions.

Along the radial direction, the design pitch is 1.18 mm. However this value depends strongly, not only on the mechanical process, but also on the building process of the module. Due to these reasons, after examining the cross-sectional area of the first two modules made, the values were measured as 1.24 mm pitch for the first (blue) and 1.22 mm pitch for the second (green). The matrix's density is such that the depth of the module, measured in radiation lengths is approximately 17 X_0.

This 1.24 mm-pitch configuration, termed nominal configuration, has been studied for energy resolution and fractional energy deposition quite thoroughly, first by simulations with GEANT [1–3] and also from the beam test

data [4] and the results from both methods agree.
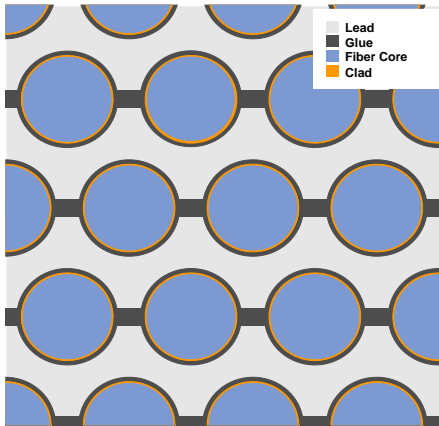
Fig. 2. Module's x-y cross-sectional area

2 Motivation

The GlueX detector is based on a superconducting solenoid with a 2.2 Tesla central field. The BCAL resides inside this magnet and therefore must employ a readout photo sensor capable of this field. Silicon photo multipliers (SiPM) are leading contenders for the readout, but the technology currently available limits their photon detection efficiency to $\sim 10\%$. These devices could clearly benefit by having more light incident upon them.

For particles entering the BCAL with energies more then 100 MeV, there is no issue. Particles that have energies as low as 40 MeV, on the other hand, deposit most of their energy in the first few centimeters of the inner segments of the module. In addition, light attenuation inside the fibers, further reduces the amount of light reaching the surface of the SiPM. Therefore it is straightforward to understand that the more energy a particle deposits in the sensitive material the more accurately this particle's energy can be measured by the SiPM.

This can be achieved by trading lead for scintillating fiber, or in other words, using more scintillating fibers and reducing the lead sheet's thickness. This would lead to a higher fractional energy deposition. On the other hand more scintillating fiber and less lead means reduced density of the module thus in turn radiation lengths and finally reduced capability of the module to absorb energy for energetic particles ($> 400\ MeV$) at normal incidence to the module. Indeed, for such particles a significant amount of energy leaks from the back of the calorimeter and thus degrades the BCAL's energy resolution. This is no

concern for low energy particles, as the module is still thick enough to absorb all of their energy.

Different configurations of the geometry of the BCAL can optimize both desired goals. First, to capture as much energy of the higher energy particles and second for low energy particles to have the best possible ratio of energy deposited in the scintillating fibers over the amount of energy deposited in the non sensitive materials of the BCAL.

3 Description of Setup

3.1 Geometrical configuration

Three geometry configurations were simulated.

- nominal geometry with radial pitch of 1.24 mm.
- light geometry with a resulting radial pitch of 1.11 mm.
- hybrid geometry is a mixture of nominal and light geometry.

The light geometry is made of thin lead sheets and the result is a radial pitch of 1.11 mm. In the hybrid geometry the first 6 cm (first 3 segments), were made of the thin 1.11 mm pitch lead sheet geometry and the rest (6 cm to 22.5 cm) were made of the nominal geometry of 1.24 mm pitch. Additional simulations where carried out using other thicknesses but were not pertinent to this study and therefore not reported here. Thinner lead sheets impact

(a) 1.24 mm radial pitch of fibers.   (b) 1.11 mm radial fiber pitch.
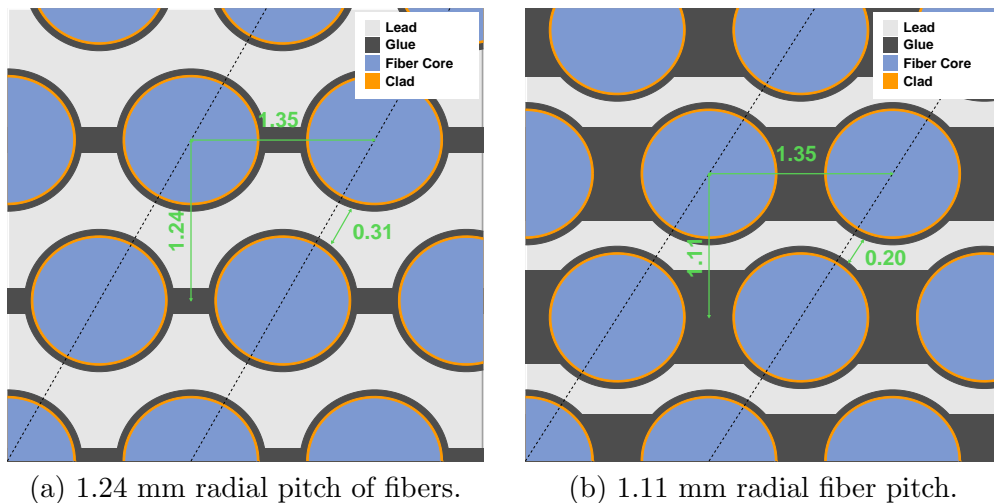
Fig. 3.

the detailed geometry view of Figure 2. By using knowledge from the KLOE

4

calorimeter prototypes the following observations on the behavior of the lead sheets can be drawn. When the lead sheets are thick enough, about 0.5 mm, the swaging process is very precise in formulating the place where each fiber will be glued. When the lead sheet thickness decreases, there is not enough material for the grooves to be well formulated. Instead what happens is the lead sheet only takes a wavy form, and most of the space between fibers is now covered by glue. These configurations are shown in Figures 3a and 3b. In all simulations, cladding has been added to the fibers, thus reducing the fiber core diameter to 4% smaller diameter than the nominal simulations, because the BCAL will employ double-clad fibers.

3.2   Calculation of radiation length (X_0)

Each module consists of three different elements: lead, fiber and glue. The radiation length is given by

$$\frac{1}{X_0} = \sum_j \frac{w_j}{X_j} \tag{1}$$

where w_j is the fraction by weight and X_j is the radiation length of the jth element. There are several ways to calculate X_j for the three elements of interest [5]. Table 1 summarizes all the data for each element needed to calculate the radiation length (X_0) for each of the geometries used in the simulations, which are shown in Table 2.

Element	A	Z	ρ (g/cm^3)	X_j (cm)
Pb	207.2	82	11.35	0.56
SciFi	11.163	5.615	1.049	42.46
Glue	11.291	5.686	1.180	37.36

Table 1
Information for the materials comprising the module.

3.3   Simulation Code

To answer the questions set in the previous section a series of simulations have been done using GEANT. The Fortran code, used to simulate the barrel calorimeter of the GlueX project, is based on the same code used to simulate the nominal geometry. However the code has been greatly altered to be more

Geometry	Element	w_j	Z_{eff}	A_{eff}	X_0 (cm)	Molière Radius (cm)
1.24 mm pitch	Pb	0.8719	72.22	182.10	1.40	3.54
	SciFi	0.0958				
	Glue	0.0323				
1.11 mm pitch	Pb	0.7290	61.31	154.09	2.59	5.57
	SciFi	0.1691				
	Glue	0.1019				

Table 2

X_0 and the Molière Radius calculated for the nominal geometry of 1.24 mm radial pitch and the thin lead geometry of 1.11 mm radial pitch.

Geometry	Front part (X_0)	Rear part (X_0)	Total (X_0)
1.24 mm pitch	-	-	16.87
1.11 mm pitch	-	-	9.34
hybrid	2.43	12.48	14.91

Table 3

Width of the module expressed in radiation length units. The hybrid module is made of a 1.11 mm pitch inner part of thickness 2.43 X_0. The outer part has 1.24 mm pitch and is 12.48 X_0 thick.

efficient and easy to customize: most of the critical data about geometry used by GEANT to construct the BCAL module have been transferred into data cards. New functionality has been also added: simulations of modules with different lead sheet thickness and/or different lead sheet thickness for the inner layers versus the outer layers can be done easily by making appropriate changes to the data card.

Using GEANT, we used two different ways to implement the geometry for the simulation. The first consists of making the glue boxes look like small trapezoids between the fibers and the second consists of strips of glue placed inside the lead and on top of them the fibers. To distinguish one from the other, we will be calling the first one *traps* Figure 4a and the second *strips* Figure 4b.

(a) *traps* implementation.   (b) *strips* implementation.
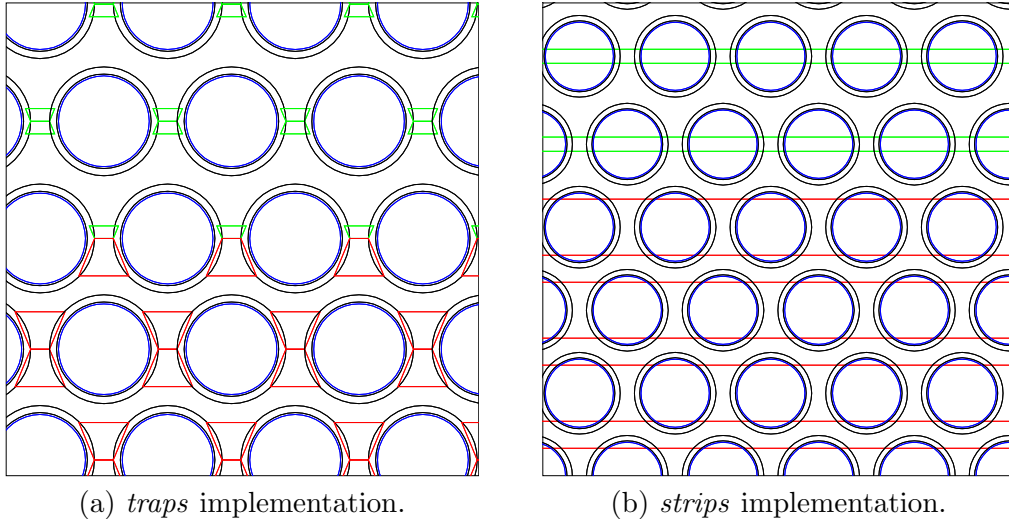
Fig. 4. Different implementations of the various geometries.

4 Results

Simulations have been carried out for various angles in respect to the beam, as well as many different energies and all geometries listed above. The goal was to extract the longitudinal shower profile, the energy resolution (σ_E/E) and the fractional energy deposition (f) for each geometry.

4.1 Longitudinal Shower Profile

The parametrized longitudinal development of electromagnetic shower describes the shower well enough [5]. If the depth in the material, expressed in radiation length units is $t = x/X_0$ and the incident energy of the particle is E_0 then

$$\frac{dE}{dt} = E_0 \, b \, \frac{(bt)^{a-1} \, e^{-bt}}{\Gamma(a)} \tag{2}$$

describes the evolution of the electromagnetic cascade in the material. The parameters a and b depend on the nature of the incident particle and the type of the absorbing material. The depth in the material where the shower maximum occurs, depends on the incident particles energy E_0 and the critical energy E_c

$$t_{max} = ln\frac{E_0}{E_c} + t_0, \quad t_0 = \begin{cases} +0.5 & \text{for photons} \\ -0.5 & \text{for electrons} \end{cases} \tag{3}$$

In the case of the absorbing medium being a compound, the critical energy depends on the Z_{eff} of the compound. According to the Rossi formula [6]

$$E_c = \frac{610 MeV}{Z_{eff} + 1.24} \tag{4}$$

Equation (2) is to be used for the entire module with the appropriate Z_{eff}. However, the same curve with different parameters describes the shape of the longitudinal shower profile in the scintillating fibers only. It will be shown later that this is actually a very good assumption.

The longitudinal shower profile for different angles of the momentum of the incident photon in respect to the beam direction, as well as different incident photon energies, are shown in the set of graphs in Figures 5 and 6. The profile shown is for the energy deposited in the scintillating fibers.

The data points in each case have been fitted with the function

$$\frac{dE}{dt} = A \frac{t^B e^{-Ct}}{\Gamma(B+1)} \tag{5}$$

where A, B and C are parameters to the fit. Also by comparing Equations 2 and 5, A depends on E_0, a and b, $B = a - 1$ and $C = b$. Note that in Figure 5 the curves for the hybrid geometry exhibit the expected transition from the thinner lead in the inner layers to the thicker lead distribution at the outer layers. There is a discontinuity at that point that cannot be expressed by Equation 2.

4.2 Energy Resolution

Energy resolution is the ratio σ_E/E and it can be given as the sum in quadrature of three terms.

$$\frac{\sigma_E}{E} = \frac{a}{\sqrt{E(GeV)}} \oplus b \oplus \frac{c}{E} \tag{6}$$

The first term is called the stochastic term due to that it represents the shower fluctuations. Since the calorimeter is made of layers of fibers interleaved with lead, the number of shower particles reaching the sampling medium (fibers) has a stochastic behavior. The energy deposited in the sampling medium inherits this stochastic behavior. Increase of the sampling medium volume would reduce fluctuations thus improve the resolution. On the other hand this modification would lead to a "lighter" calorimeter with compromised ability to stop
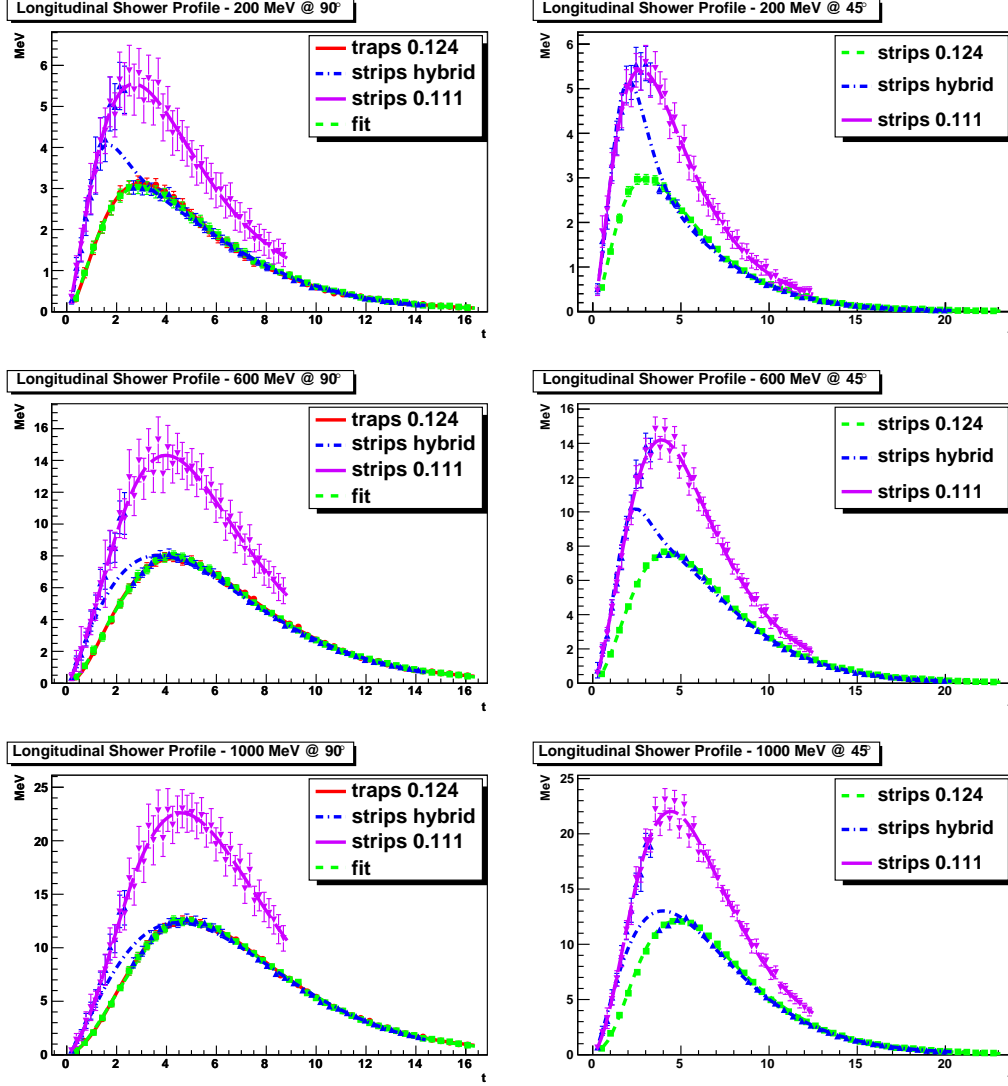
Fig. 5. Longitudinal shower profile at 90° and 45° for different implementations and geometries. The solid line at 90° shows how well the two different implementations of the geometry agree.

energy leaking from the back. It follows then that for optimal results on the resolution, for a given region of the incident particle's energy, determining the best ratio of sampling medium weight is needed. The second term, called the floor term represents the dependence on the irregularities of the lead, glue, fiber matrix that the calorimeter consists of. Finally the last term is called the noise term and depends mostly on electronics noise. Consistent with our discussion about the three terms of the resolution, the function to fit the graphs is Equation 7, $(c = 0)$.

$$\frac{\sigma_E}{E} = \frac{a}{\sqrt{E(GeV)}} \oplus b \tag{7}$$

9
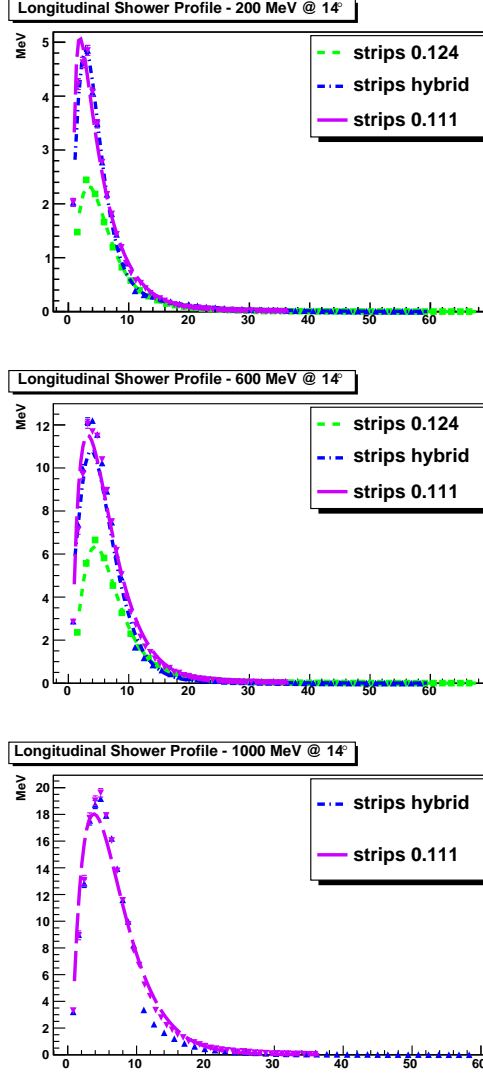
Fig. 6. Longitudinal shower profile at 14° for different geometries.

For photons at normal incidence, the results are in agreement with past simulations, including the decrease of the floor term at forward angles. Finally the resolution at 90° for the nominal and thin lead behave reasonably, with the former having a higher $\frac{1}{\sqrt{E}}$ term and better floor term than the latter. This is understood in the sense that the latter has a higher fiber volume and thus collects more of the deposited energy. That causes an improvement in the stochastic fluctuations ($\frac{1}{\sqrt{E}}$ term) where as its geometrical non uniformity leads to a worse floor term.
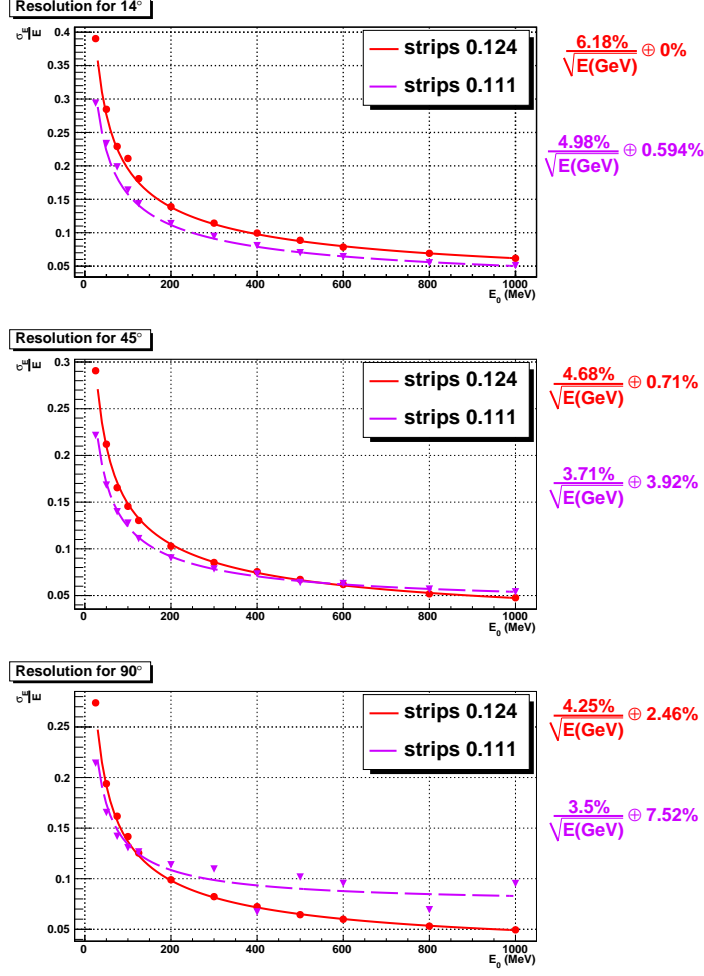
Fig. 7. Energy Resolution

4.3 Sampling Fraction

Sampling fraction is the fraction of the energy that is deposited in the sampling material (here scintillating fibers) over the total energy deposited in the module.

$$f = \frac{E_{scifi}}{E_{mod}} \tag{8}$$

It can also be expressed as the ratio of the energy deposited in the sampling material over the incident energy of the particle.

$$f_\gamma = \frac{E_{scifi}}{E_\gamma} \tag{9}$$

f_γ is always smaller than f since E_{mod} is always smaller than E_γ.

11
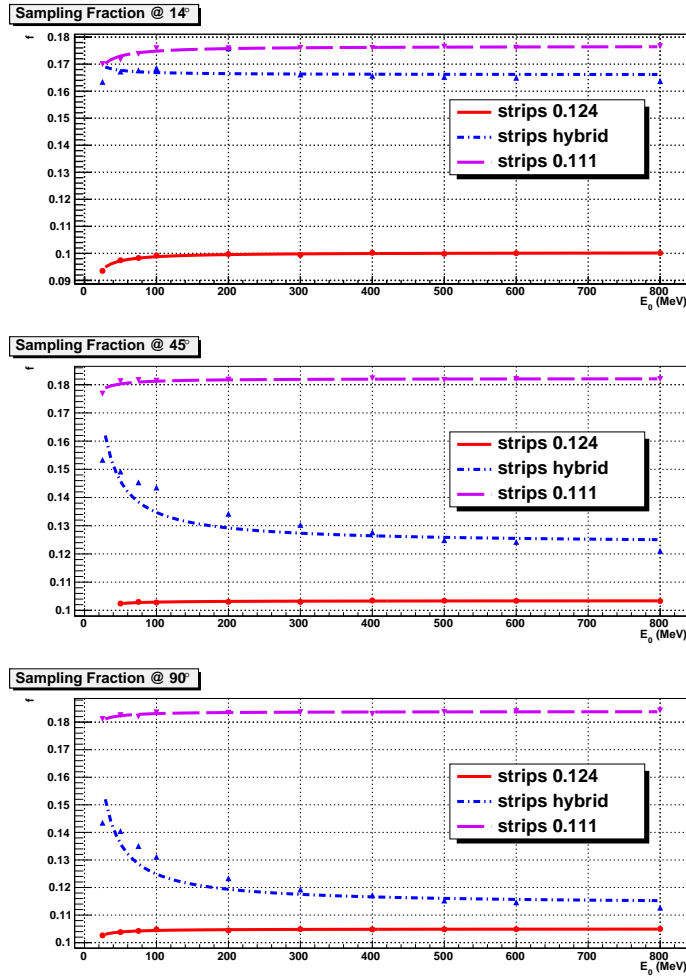
Fig. 8. Sampling Fraction for different angles. The lines are not fits but only to make it easier to estimate the fractional energy deposition in the graph.

The sampling fraction plotted as a function of the incident photon energy is shown in Figure 8. The lines are not fits; they are just there to guide the eye to an estimation of the sampling fraction. The values of teh sampling fraction are shown in Table 4. The sampling fraction for the thin lead and the nominal geometry are typically constant, especially for higher energies and agree with past studies. The hybrid geometry line reflects the increase of the fiber volume in the first segments of the module. This increase was the goal to be achieved by introducing the hybrid geometry, though it is difficult to account for the discontinuity that is introduced by the geometry configuration used.

The sampling fraction is smaller than those calculated by other studies [3,5], on the BCAL, due to the difference in the geometrical configuration, namely due to the radial pitch being changed from 1.22 mm [3] and 1.18 mm [5] to 1.24 mm, in order to better approximate the actual pitch value. Another very important change that greatly affects the sampling fraction is the reduction of the fibers core volume due to the addition of cladding. The difference is quite

12

Angle	pitch	f	f (w/o cladding)	f_γ	f_γ (w/o cladding)
	nominal	10.455 ± 0.015	11.374 ± 0.016	9.854 ± 0.015	10.721 ± 0.016
$90°$	hybrid	12.175 ± 0.023	13.255 ± 0.025	11.415 ± 0.025	12.410 ± 0.027
	thin	18.289 ± 0.023	19.878 ± 0.024	15.64 ± 0.03	17.01 ± 0.04
	nominal	10.310 ± 0.018	11.223 ± 0.019	9.700 ± 0.018	10.558 ± 0.019
$45°$	hybrid	13.46 ± 0.03	14.62 ± 0.03	12.539 ± 0.028	13.63 ± 0.03
	thin	18.196 ± 0.024	19.792 ± 0.026	16.136 ± 0.029	17.56 ± 0.03
	nominal	9.955 ± 0.022	10.834 ± 0.023	8.753 ± 0.023	9.548 ± 0.024
$14°$	hybrid	17.164 ± 0.028	18.66 ± 0.03	14.723 ± 0.028	16.000 ± 0.030
	thin	17.559 ± 0.026	19.097 ± 0.027	15.036 ± 0.028	16.37 ± 0.03

Table 4

Fractional energy deposition for various geometries and angles. The values without cladding were extracted with the energy deposited in the cladding added to the energy of the fiber's core.

significant and a closer look to the role of the cladding is described in the the next paragraph.

4.3.1 Effect of cladding on the Sampling Fraction
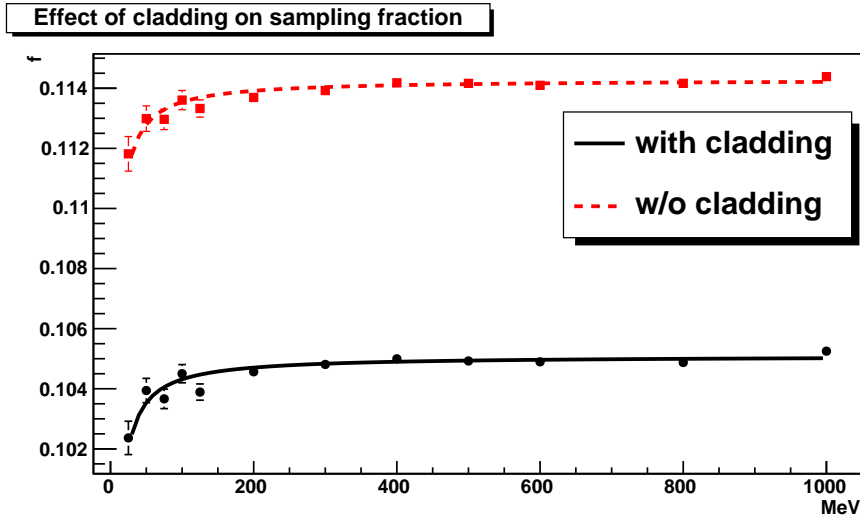
Fig. 9. Sampling fraction comparison between fibers with cladding and without cladding. The angle of incidence is 90°

As mentioned earlier, cladding around the core of the scintillating fibers has been added in these simulations. Cladding represents 4% of the total diameter of the fiber. Therefore in the simulations carried out the sampling material is less in volume than older simulations where the total diameter of the fiber

13

was contributing to the sampled energy. The difference in the volume of the fiber due to the added cladding is

$$\frac{\Delta V}{V} = \frac{\pi z \left(R^2 - 0.96^2 R^2 \right)}{\pi z R^2} = 7.84\%$$

This change in the volume of the sampling material affects the sampling fraction as shown in Figure 9. The sampling fraction without cladding and with cladding is termed f_{wo} and f_w respectively. From Table 4 $f_{wo} = 0.114$ and $f_w = 0.105$ approximately. This means there is a decrease in the sampling fraction of

$$\frac{\Delta f}{f_{wo}} = \frac{f_{wo} - f_w}{f_{wo}} \approx 7.8\%$$

As expected, the sampling fraction ratio decreases with the decrease of the volume of the sampling material. The sampling fraction is approximately 11.4% without the addition of cladding, which is in very good agreement with the results from older simulations of the BCAL [3]. However the 10.5% is more accurate because of the cladding taken into account.

5   Energy Leakage

The energy leakage for normal incidence [1] and all the different radial pitch configurations is shown in Figure 10. The different curves correspond to energy leaking out from different faces of the module. Front and back refers to the inner and outer face of the module, respectively, with respect to the radial direction. Leakage from the sides refers to the faces of the module that will be in touch with it's nearest neighbor modules and leakage from the ends refers to the energy leaking out from the faces of the module along the direction of the beam, on which photo sensors eill be placed. Finally total energy leakage is referred to the sum of all the energy that leaked out of the module regardless of the face were the leak occurred.

In this study energy from the sides has been treated as leak, in the sense that it is not detected. However, when the 48 modules are put together to form the entire BCAL, the energy coming out of the sides of one module will be deposited to the modules next to it. For incident photon angles of $90°$, leaking occurs mostly from the back of the module. At normal incidence the module's radial thickness, was previously calculated and is shown in Table 3. As the radial thickness of the module decreases, due to the change in pitch,

---
[1] See section A in page 17, for energy leakage for angles other than normal.
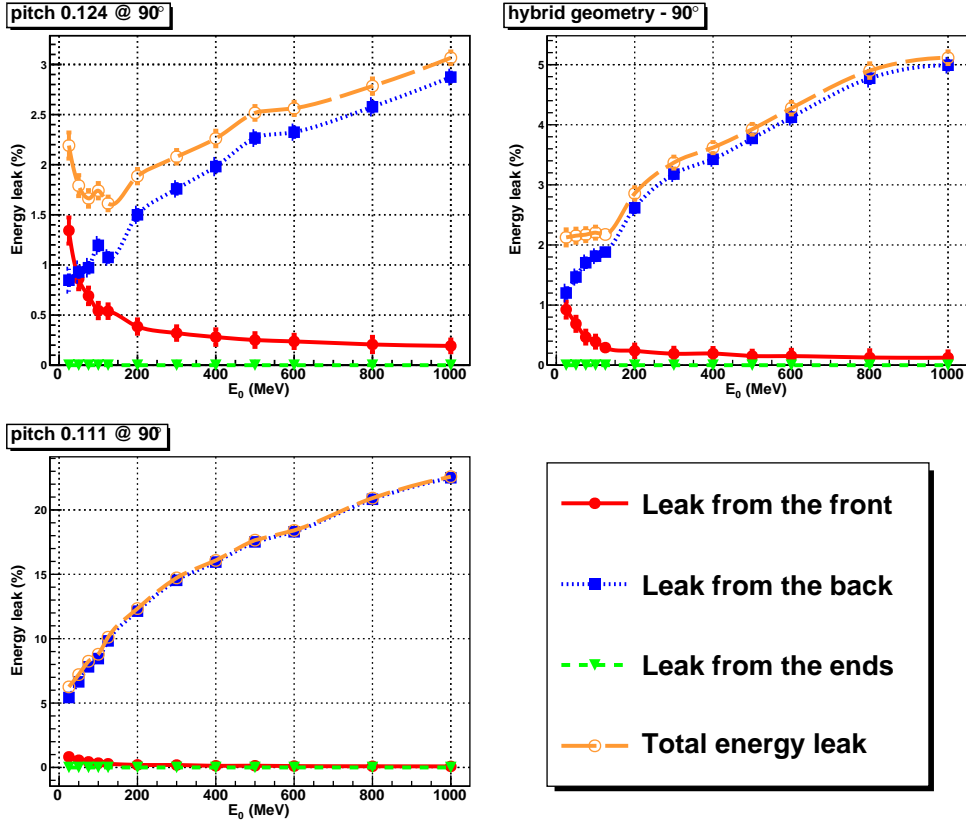
Fig. 10. Energy leaking out of the module for different energies and incident angles.

more energy leaks from the back. It is interesting to notice that the amount of energy leaking out from the sides is in the order of magnitude of the energy leaking from the back. The Molière radius for the thin lead geometry is 5.57 cm and for the nominal 3.54 cm. For the thin geometry, the Molière radius is larger than the thickness of the module. This justifies the increased leakage from the sides of the module in the thin geometry.

There is very little energy leaking from the ends and the front face of the module. Even at 14° energy leakage from the ends is negligible because of the absorption of the energy by the inner segments of the module. Energy is absorbed in the first inner segments of the module, before it reaches the rear front corner of the module,for incident angles as low as 14°.

6   Conclusions

The nominal geometry has been tested once again with the GEANT based, standalone Monte Carlo. The extraction of the critical parameters such as energy resolution and fractional energy deposition have been extracted in very good agreement with older simulations. Moreover these new results reflect the

more accurately calculated radial pitch fiber, which has been found to be closer to 1.24 mm. Also the addition of cladding has been shown to have a significant affect. Going to a new geometry with thinner lead sheets such that the resulting fiber pitch is 1.11 mm, leads to increased sampling fraction and lower energy resolution. The energy leakage though is significantly increased. Such a choice of geometry would be beneficial, if the energy of the incident particles was expected to be low.

The specifications under which the BCAL is being constructed and anticipated to operate, make such a choice void, mainly in the sense that the timetable of the BCAL did not allow for the R&D required to swage thin lead. It was decided within GlueX to not pursue the thin or the hybrid designs further. Moreover since the initiation of this study it has been decided that the SiPMs are going to be cooled down to +5 °C, thus reducing the dark current and increasing their photon detection efficiency. The higher gain of the SiPM can be achieved by operating the device at higher bias, allowed by the cooling and therefore not requiring a change in the geometry of the calorimeter itself .

7 Acknowledgments

A Energy leakage for different angles

Below are the energy leak graphs for angles of incidence other than perpendicular. Figure A.1 and figure A.2 show the energy leak for angle of incidence 45° and 14° respectively. Due to the configuration of the target in respect to the BCAL, it is expected that photons with incident momentum of 14° with respect to the beam line, will hit the forward rear corner of the BCAL. At this angle, photons will encounter the most material possible, approximately of thickness 67 X_0.
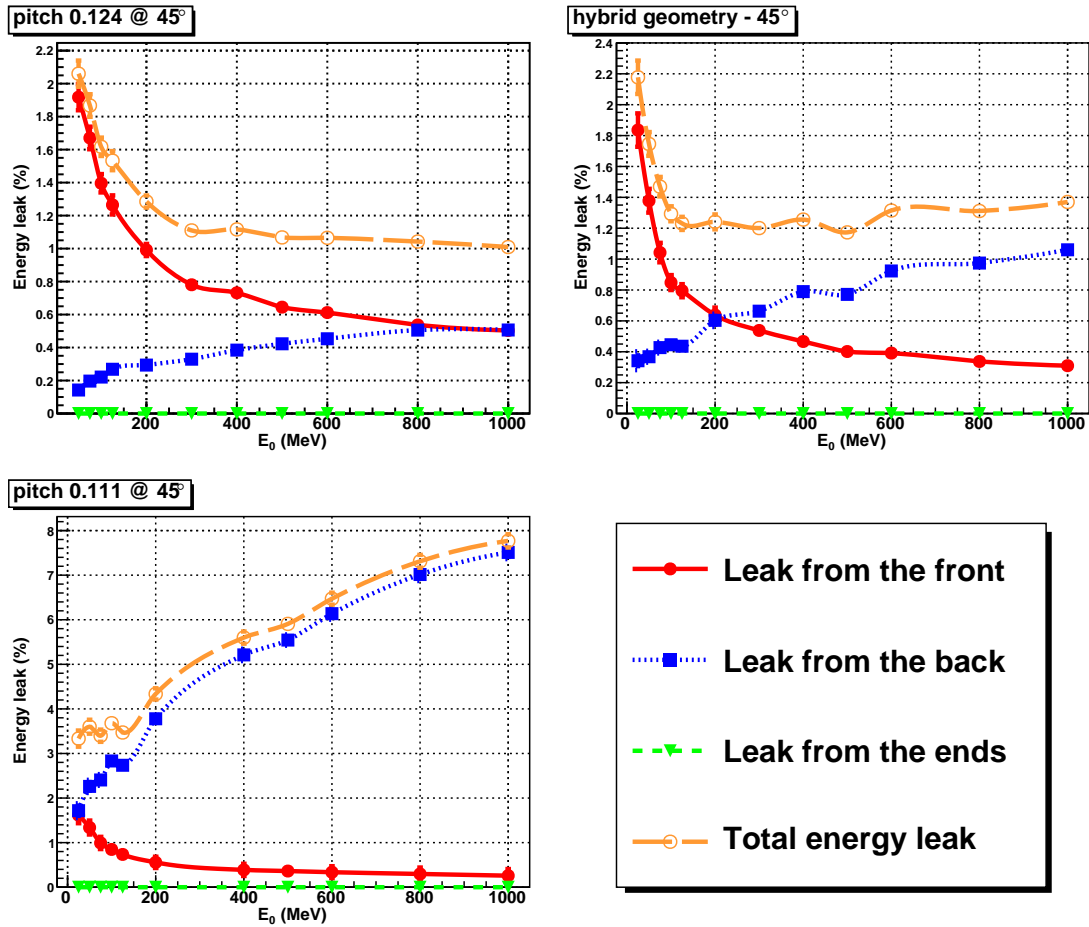
Fig. A.1. Energy leakage at 45° angle of incidence.
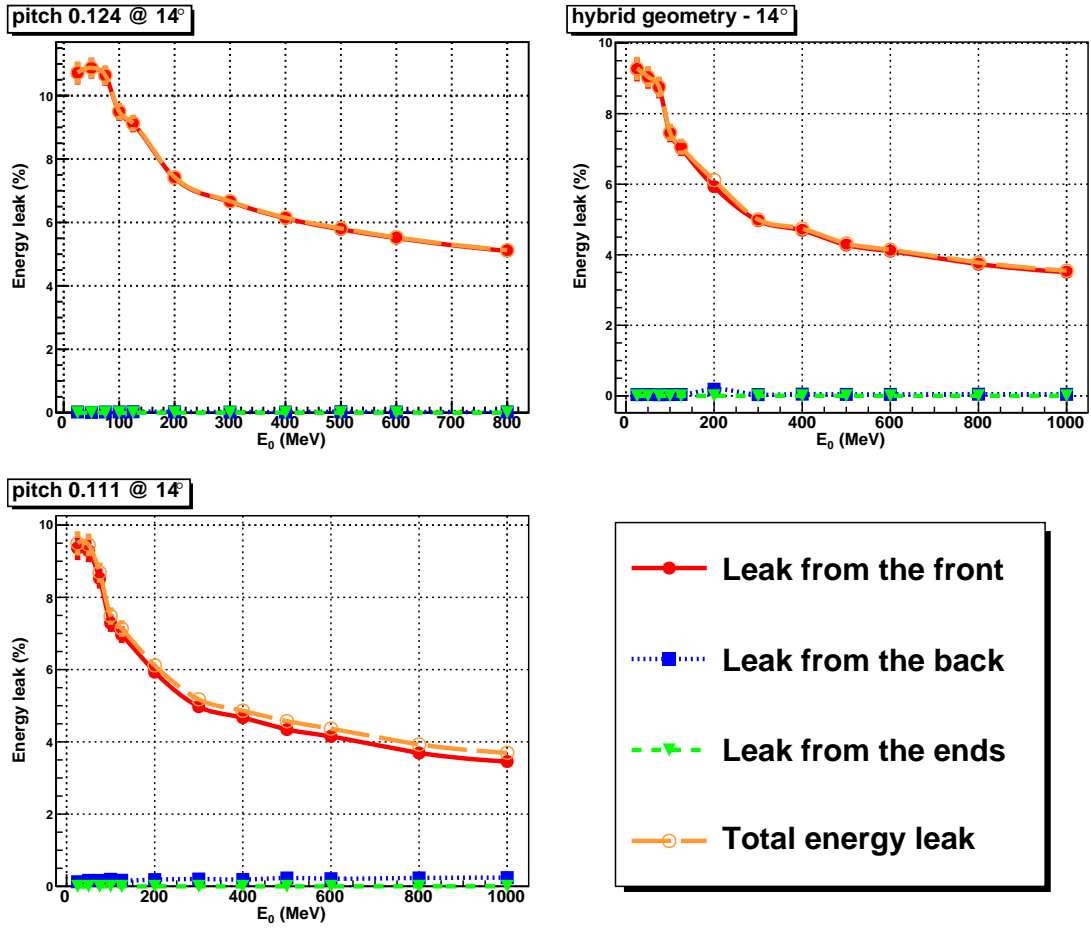
Fig. A.2. Energy leakage at 14° angle of incidence.

References

[1] R. Hakobyan, Z. Papandreou, G. Lolos, and B. Leverington. BCAL simulations for the Hall B tests. Technical report, GlueX Collaboration, 2007. GlueX-doc-796-v1.

[2] R. Hakobyan et al. BCAL energy leakage simulations. Technical report, GlueX Collaboration, 2007. GlueX-doc-797-v1.

[3] B. Leverington. Sampling fraction fluctuations. Technical report, GlueX Collaboration, 2007. GlueX-doc-827-v3.

[4] B. Leverington. Analysis of the BCAL beam tests. Technical report, GlueX Document, 2007. GlueX-doc-804-v4.

[5] Z. Papandreou. BCAL calorimetry response. Technical report, GlueX Collaboration, 2007. GlueX-doc-840-v2.

[6] B. Rossi. *High Energy Particles*. Prentice-Hall, Inc., Engelwood Cliffs, NJ, 1952.